

Geologic Studies of Planetary Surfaces Using Radar Polarimetric Imaging

Geologic studies of planetary surfaces by the world's largest radar, using polarimetric imaging, are discussed in this paper.

By LYNN M. CARTER, DONALD B. CAMPBELL, AND BRUCE A. CAMPBELL

ABSTRACT | Radar is a useful remote sensing tool for studying planetary geology because it is sensitive to the composition, structure, and roughness of the surface and can penetrate some materials to reveal buried terrain. The Arecibo Observatory radar system transmits a single sense of circular polarization, and both senses of circular polarization are received, which allows for the construction of the Stokes polarization vector. From the Stokes vector, daughter products such as the circular polarization ratio, the degree of linear polarization, and linear polarization angle are obtained. Recent polarimetric imaging using Arecibo has included Venus and the Moon. These observations can be compared to radar data for terrestrial surfaces to better understand surface physical properties and regional geologic evolution. For example, polarimetric radar studies of volcanic settings on Venus, the Moon, and Earth display some similarities, but also illustrate a variety of different emplacement and erosion mechanisms. Polarimetric radar data provide important information about surface properties beyond what can be obtained from single-polarization radar. Future observations using polarimetric synthetic aperture

radar will provide information on roughness, composition, and stratigraphy that will support a broader interpretation of surface evolution.

KEYWORDS | Moon; polarimetry; radar; Venus

I. INTRODUCTION

Radar polarimetry has the potential to provide more information about surface physical properties than single-polarization backscatter measurements, and has often been used in remote sensing observations of Solar System objects. Many pioneering dual-polarization studies utilized ground-based radio telescopes and radar systems, in part because early Earth-orbital and planetary sensors were constrained in sensitivity or downlink data rate. For example, the radar on the Magellan mission to Venus measured only horizontally (H) polarized radiation, except for a few orbits where the spacecraft was rotated to measure the vertical (V) polarization. The Cassini radar also images in a single polarization. The recent Mini-RF (radio frequency) radars on Chandrayaan-1 and the Lunar Reconnaissance Orbiter, using a hybrid-polarity architecture to generate the Stokes vector [26], [28], mark the first time that such imaging radar data have been obtained from a planetary mission.

The first radar polarimetric studies of Venus employed a system that transmitted one circular polarization and received two orthogonal circular polarizations [25]. This allowed for the first measurements of the ratio of the circular polarizations and enabled scattering law comparisons. Comparing spectra of Venus in both circular polarization channels allowed the identification of comparatively rough

Manuscript received March 2, 2010; revised September 9, 2010; accepted November 19, 2010. Date of publication February 10, 2011; date of current version April 19, 2011. Arecibo Observatory is part of the National Astronomy and Ionosphere Center, which is operated by Cornell University under a cooperative agreement with the National Science Foundation (NSF). The GBT is part of the National Radio Astronomy Observatory, a facility of the NSF that is operated under cooperative agreement by the Associated Universities, Inc.

L. M. Carter is with the Planetary Geodynamics Lab, NASA Goddard Space Flight Center, Greenbelt, MD 20771 USA (e-mail: lynn.m.carter@nasa.gov).

D. B. Campbell is with the Department of Astronomy, Cornell University, Ithaca, NY 14853 USA (e-mail: campbell@astro.cornell.edu).

B. A. Campbell is with the Center for Earth and Planetary Studies, Smithsonian Institution, Washington, DC 20013-7012 USA (e-mail: campbellb@si.edu).

Digital Object Identifier: 10.1109/JPROC.2010.2099090

surface features that appeared at specific rotational phases [15], [20]. The diffuse scattering behavior appeared similar to that observed for the Moon, but the quasi-specular component was stronger and exhibited a steeper drop with incidence angle, indicative of smaller surface slopes [15]. Hagfors and Campbell [22] observed Venus using the 70-cm wavelength radar at Arecibo and measured cross section, circular polarization ratio, and the fraction (degree) of linear polarization in the received echo versus incidence angle along the apparent rotation axis (time delay). The degree of linear polarization was much lower than corresponding lunar values, which suggested less surface penetration of the radar wave on Venus.

Studies of the Moon have also long employed polarimetry as a means to understand surface composition and structure. Many experiments revealed that the total echo power received in the same sense circular polarization as was transmitted is about 13 dB below that received in the opposite sense circular polarization (for example, see [14]). Hagfors *et al.* [23] used the Millstone Hill 23-cm wavelength radar to investigate the nature and distribution of the lunar regolith covering. A circular polarization was transmitted and two orthogonal linear polarizations were received; the resulting frequency spectra and polarization ratios were consistent with a tenuous tens-of-centimeters-thick surface layer [23]. Evans and Hagfors [16] measured the backscatter behavior of linear-polarized waves using a specially constructed polarizer at Millstone Hill, also at 23-cm wavelength. They found that in the diffuse region of echoes (incidence angles greater than 40°) only 1/8 of the total power is returned in the linear mode orthogonal to that transmitted, suggesting that either multiple reflections can occur or that the echo is partially reflected from the subsurface. Zisk *et al.* [36] acquired dual-circular polarization data of the Moon at 3.0-cm wavelength using Haystack Observatory. These data were used to study the scattering properties of the Apollo 15 landing site [36] and to measure surface properties around lunar impact craters [1], [2]. Stacy [29] used the 12.6-cm radar system at Arecibo to search for possible evidence of ice at the lunar poles [30], [31]. Images of Sinus Iridum and Mare Imbrium were used to investigate scattering from the mare, and a comparison of the fraction of linear polarized echo power to models showed that some of the backscattered power must come from subsurface quasi-specular scattering [29].

Over the past decade, improvements to ground-based telescope facilities, including a higher powered Arecibo Observatory radar, improved receivers, and new fast-sampling instruments, have allowed full Stokes vector radar imaging of the inner Solar System at higher resolution than was previously possible. These new capabilities provide the opportunity to use radar polarimetry to study geology at local to regional scales. In particular, radar polarimetry has been used to study volcanism, impact cratering, and surface properties on Venus and the Moon (e.g., [8], [9], [12], [13], [18], [31], [32], and [35]), which are

both relatively close to Earth and yield high signal-to-noise ratio data. Planetary radar data can also be compared to imaging radar observations of terrestrial-analog settings to better understand the observed scattering behaviors. Cross comparisons of the available data sets demonstrate that radar polarimetry is useful for discriminating between different types of geologic surfaces and mantling cover. Below, we use radar data obtained and analyzed over the last several years to compare the scattering behaviors of similar terrain types on Venus, the Moon, and Earth. This is the first time that relatively high-resolution polarimetric radar imaging has been available for such a cross-planet comparison. These comparisons elucidate the range of observed scattering behaviors and identify puzzling cases that have no clear physical explanation based on current models.

II. DESCRIPTION OF POLARIMETRIC DATA PRODUCTS

Ground-based radio telescopes are typically able to receive two orthogonal polarizations simultaneously, and from these data it is possible to create the Stokes vector. The data described below were obtained using the Arecibo Observatory 12.6-cm wavelength (S-band) radar system as a transmitter, and either Arecibo or the Robert C. Byrd Green Bank Telescope (GBT) as the receiver. The Arecibo radar transmits a circular polarization, and both Arecibo and the GBT can receive two orthogonal circular polarizations, referred to as the same-sense circular (SC) and opposite-sense circular (OC) polarizations (to that transmitted). Fully polarimetric observations were not used because typically the radar transmits continuously. In the past, when pulsed waveforms were used, suitable switches that would permit transmit polarization switching were not available at the power levels used (typically hundreds of kilowatts).

In the case of Venus, the beam of the Arecibo telescope at S-band is two arcminutes, which is about twice the angular size of Venus at closest approach to Earth. To reduce the resulting north-south delay-Doppler ambiguity problem, we pointed north and south of the planet on alternating radar runs to allow the central portion of the beam to preferentially illuminate one hemisphere. The resulting images therefore contain echo power from the entire Earth-facing hemisphere of Venus. The Venus data were mapped to a Mercator projection that shows either the north or south (depending on the telescope pointing), with areas near the Doppler equator excluded. The incidence angle variation across the surface is due to both the curvature of the spherical planet and to changes in topography. However, when looking at the global maps at low (~ 12 km) resolution, the largest changes in incidence angle are from the curvature of the planet. For the lunar observations, the Arecibo beam subtends only a small portion of the lunar surface, and there is no ambiguity except in areas near the Doppler equator.

Incidence angle variation within a given lunar image can be dominated by local topography, although this depends on the particular subradar point and the amount of local topographic variation.

In both the Venus and lunar cases, the received data are converted into complex-valued delay-Doppler images, and a relative channel balance is applied based on background noise measured off-planet. The delay-Doppler maps are converted into latitude/longitude format, which includes focusing for the lunar case [7]. The maps are then converted into real-valued Stokes vector images, and daughter products such as the circular polarization ratio are computed. Additional discussion of observational parameters and data processing can be found in [12] and [9]. Below, we describe the daughter products in more detail.

The Stokes vector generated from the received circular polarizations can be used to completely describe the polarization state of the received wave [24]

$$S = \begin{bmatrix} S_1 \\ S_2 \\ S_3 \\ S_4 \end{bmatrix} = \begin{bmatrix} \langle |E_L|^2 \rangle + \langle |E_R|^2 \rangle \\ 2\text{Re}\langle E_L E_R^* \rangle \\ 2\text{Im}\langle E_L E_R^* \rangle \\ \langle |E_L|^2 \rangle - \langle |E_R|^2 \rangle \end{bmatrix} \quad (1)$$

where E_L and E_R are the electric fields for the left and right circular polarizations, respectively, and the averages are time or spatial averages. In practice, (1) is used to derive the Stokes parameters using fully processed OC and SC complex-valued images. The first Stokes parameter (S_1) is a measure of the total average power in the echo. The S_2 and S_3 Stokes parameters describe the linearly polarized state of the wave. The S_4 Stokes parameter gives the direction and magnitude of the circularly polarized power.

There are two particularly useful daughter products that can be derived from the Stokes vector: the circular polarization ratio ($\mu_c = \text{SC/OC}$) and the degree of linear polarization (m_l). The circular polarization ratio can be used as an indicator of surface roughness. Specular echoes from surfaces that are smooth at wavelength scales will lead to low ratios, while diffuse scattering from rough surfaces generates μ_c values approaching one, or even greater than one for extremely rough terrain and low-temperature water ice when it is present. The circular polarization ratio can be calculated from

$$\mu_c = \frac{S_1 - S_4}{S_1 + S_4}. \quad (2)$$

The circular polarization ratio will tend to increase with incidence angle because near-nadir scattering is primarily

quasi-specular (i.e., dominantly OC). At larger incidence angles, diffuse scattering generally contributes a greater fraction of power to the received echo, which leads to a higher SC/OC ratio.

For a circular-polarized transmit and receive system such as Arecibo, sources of error in the circular polarization ratio are dominated by uncertainties in the relative channel gains of the OC and SC channels. In most cases, the noise background can be measured from areas of noise in off-planet areas of each image. It is important that the dynamic range of the data be well captured by the quantization; for example 4–8-b sampling has proved better than 2-b sampling for planetary targets with a large range in echo power (e.g., Moon). Otherwise, it may not be possible to obtain accurate measurements of the noise floor in each channel. During processing, the data are divided by the noise measurements to balance the channels. Typically, and for the data shown below, a very good channel balance can be achieved, and the resultant uncertainty in μ_c values is small (a few percent).

The linear-polarized component of the received echo can be used to infer the presence of subsurface scattering. A circularly polarized incident wave can be thought of as a combination of two orthogonal linear vectors that are vertically (V) and horizontally (H) polarized with respect to the plane of incidence. These two components have different power transmission coefficients [24]

$$T_H(\theta, \epsilon') = \frac{4 \cos \theta \sqrt{\epsilon' - \sin^2 \theta}}{(\cos \theta + \sqrt{\epsilon' - \sin^2 \theta})^2} \quad (3)$$

$$T_V(\theta, \epsilon') = \frac{4\epsilon' \cos \theta \sqrt{\epsilon' - \sin^2 \theta}}{(\epsilon' \cos \theta + \sqrt{\epsilon' - \sin^2 \theta})^2} \quad (4)$$

where θ is the angle between the surface normal and the incoming radar wave (incidence angle) and ϵ' is the real component of the dielectric constant. If this wave penetrates the surface, the V polarization will be preferentially transmitted, and the polarization state will change from circular to elliptical. The reflected wave exiting the surface towards the radar will experience a similar preferential transmission of the V polarization component. The elliptical polarization can be thought of as a combination of circularly polarized power and a linear component with a measurable magnitude and direction. The degree (or percent) of linear polarization is

$$m_l = \frac{\sqrt{S_2^2 + S_3^2}}{S_1}. \quad (5)$$

The long axis of the polarization ellipse indicates the direction of the linear polarization vector. The angle of this

major axis, with respect to H polarization, is given by

$$\chi = \frac{1}{2} \arctan\left(\frac{S_3}{S_2}\right). \quad (6)$$

For subsurface scattering, the direction of the linear polarization will be parallel to the plane of incidence and reflection (a plane that includes the direction of the incident or reflected wave and the normal to the surface). The linear polarization angle will change as the surface tilts in the azimuth direction with respect to the radar. Measurements of the linear polarization angle can assist with interpretation of the degree of linear polarization; scattering from the subsurface should produce linear polarization angles that vary across the scene as the local surface normal varies with topography and the curvature of the planet. Linear polarization angles have also been used to measure local slopes [29], [30].

There are three primary sources of error in measurements of the degree of linear polarization as measured from a circular-polarized transmit and receive system: instrumental cross coupling between the circular polarizations, statistical fluctuations in the S_2 and S_3 images that create a spurious degree of linear polarization when they are squared and added, and errors in subtracting the noise background in the S_1 image. These errors are discussed in detail in [12]. Instrumental cross coupling at S-band is low for both the Arecibo and the Green Bank Telescope systems, and contributes a spurious degree of linear polarization of ~ 0.04 . The statistical background in the S_2 and S_3 images depends on the amount of spatial averaging in a given image, but the added spurious degree of linear polarization ranges from 0.02 to 0.04 in the Venus data. Errors in the S_1 background power measurement usually range from a few to several percent, which results in an added spurious linear polarization of 0.02 for a degree of linear polarization value of 0.35.

The value of m_l depends on surface physical properties (the dielectric constant and relative amounts of surface versus subsurface scattering), the radar viewing geometry with respect to the surface topography (incidence angle), and the amount of spatial averaging across surfaces with differing amounts of radar penetration. The degree of linear polarization increases with incidence angle and is zero at normal incidence. The m_l value will also be higher if the surface permittivity (ϵ') is higher, because the transmission coefficients lead to a greater difference in H and V transmitted power. However, an increase in permittivity also increases the fraction of power that is reflected directly from the surface and reduces the amount of power transmitted into the surface. For terrestrial planet surfaces, the viewing geometry is well understood. However, the spatial variation in terrain within a pixel, the dielectric properties, and the amount of power reflected

from the surface and subsurface, are generally unknown. Other data sources, such as higher resolution optical images, and laboratory measurements of dielectric properties, can be used to estimate reasonable values in some cases.

Changes in μ_c and m_l can be used to infer differences in the surface and subsurface materials and structure. As described by Stacy [29], the backscattered radar wave can be modeled using a simple single layer model with four components: surface quasi-specular scattering (σ_{qs}), surface diffuse scattering (σ_d), subsurface quasi-specular scattering (σ'_{qs}), and subsurface diffuse scattering (σ'_d). The power returned from the subsurface depends on the depth to any subsurface scatterers, their total cross section, and the loss tangent of the medium. The absolute backscatter values also depend upon the incidence angle, the dielectric constant of the surface material, and the surface roughness properties.

It is possible to compare in a relative sense the expected μ_c and m_l values for different values of the four backscatterer components, assuming that the viewing geometry and dielectric properties of the materials are similar. This approach leads to some endmember cases shown in Fig. 1, where the left-hand side shows smooth surfaces with various types of subsurface scattering, and the right-hand side shows cases where the surface echo comes primarily from diffuse scattering on surfaces that are rough at the wavelength scale.

Surface and Subsurface Scattering Scenarios

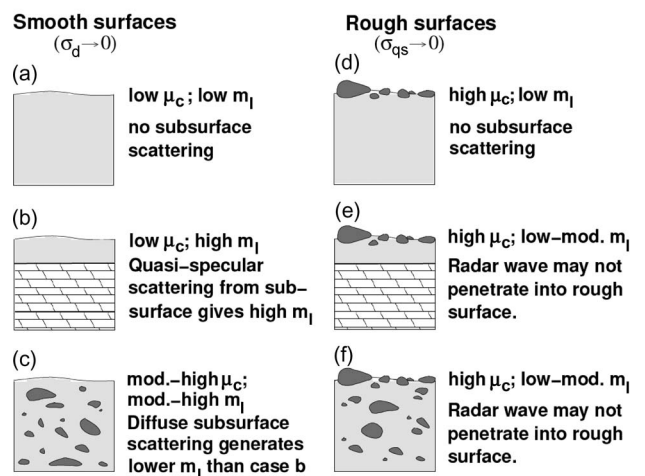


Fig. 1. Scattering endmember cases for smooth and rough surfaces, and smooth and rough subsurface reflectors. Smooth surfaces (left column) are more likely to allow for surface penetration of the radar wave. In the case of rough surfaces, the fraction of the received echo that comes from the subsurface will partially depend on the extent of the wavelength scale surface roughness. In all cases, to produce a linearly polarized echo component, the loss tangent of the mantling layer or medium must be low enough to allow the radar wave to travel far enough to reflect from buried scattering surfaces.

Although real surfaces will be some combination of these cases, the endmembers provide a basis for understanding how μ_c and m_l can change in different geologic settings. For example, areas that have a low abundance of wavelength-scale subsurface scatterers within the penetration depth of the radar, or that have a gradual change in dielectric constant with depth, will have a low degree of linear polarization [Fig. 1(a) and (d)]. Very rough crater walls and ejecta will have a high μ_c value, but a low m_l value [Fig. 1(d)]. Fine-grained deposits (e.g., impact ejecta and ash) that contain embedded rocks will produce a high m_l value [Fig. 1(c)], and they may also have a high μ_c value if a substantial amount of the echo power comes from subsurface diffuse scattering off blocks. It is usually not possible to distinguish between these schematic cases solely based on the polarization measurements. For example, it can be difficult to distinguish between different types of subsurface scattering [e.g., between Fig. 1(b) and (c) or Fig. 1(e) and (f)] unless there is other evidence to infer a buried near-planar interface or buried rocks. For example, it may be possible to determine from other remote sensing techniques that there is a buried lava flow that would lead to cases shown in Fig. 1(b) or (e). But without this information, it can be impossible to differentiate between similar endmembers, particularly because attenuation in the surface layer is unknown.

In cases where the measured μ_c and m_l values can be combined with information about the geologic setting derived from radar, optical, and infrared images, it is sometimes possible to make reasonable assumptions about the types of scattering present and thus derive a physical model. Such models can be used to compute dielectric constants, make depth estimates for mantling deposits, investigate the amount of surface versus subsurface scattering, and search for areas that are rock poor at the wavelength scale [6], [8], [29]. However, in many cases, there are simply too many uncertainties to derive unique quantitative values through modeling. This is particularly true for the Venus data shown below, where the resolution is of order ten kilometers, and it may not be a good assumption that each pixel has a uniform surface type. In these cases, a qualitative comparison between geologic units can still provide valuable information that cannot be obtained using single polarization radar data.

III. EARTH

Polarimetric radar observations of planetary analogs are useful for understanding the endmember scenarios described above. The National Aeronautics and Space Administration Jet Propulsion Laboratory (NASA/JPL) AIRSAR system collects the full 4×4 Stokes scattering operator [5], [34], which can be used to derive the daughter products discussed above. In this section, we focus on an analysis of the degree of linear polarization because it provides useful context for explaining some of the polariza-

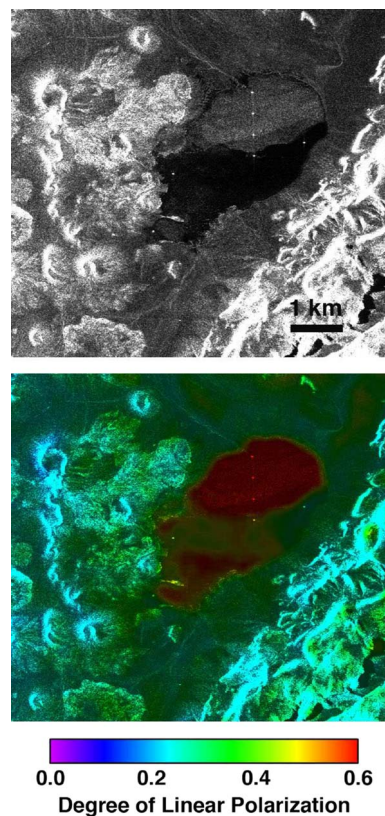


Fig. 2. AIRSAR L-band data (24-cm wavelength) of the Lunar Lake playa, in the Lunar Crater volcanic field in Nevada. North is toward the top of the images. Top: Total power image. Bottom: Corresponding color overlay of the degree of linear polarization showing high values associated with the playa.

tion behavior explored on Venus. All the study areas contain little to no vegetation, since tree trunks and shrubs will change the polarization signature.

In many AIRSAR images examined to date, a high degree of linear polarization appears to be produced when the radar wave travels into a smooth surficial layer and reflects from a buried interface that is also smooth at the wavelength scale. One such example is smooth sand deposits in the Stovepipe Wells region of Death Valley, CA [12], where the radar wave penetrates a few centimeters of sand to reflect from a buried mud-cracked surface. Another example is the Lunar Lake playa deposit in Nevada. Fig. 2 shows 24-cm AIRSAR data for Lunar Lake. The playa has a silty-clay surface with mud cracks and localized gravel patches [21]. The radar data show high m_l values (up to 0.6) across most of the playa, and very low m_l values from the surrounding rough mountains. In this case, the radar wave is likely penetrating the silt surface coating and reflecting from a buried horizon with a higher dielectric constant than the silt.

Although the geologic setting is different, a similar physical scenario (reflection from a smooth buried

interface) appears to occur in areas of smooth, ponded flows in and around the Kilauea caldera in Hawaii. In this case, near-surface air gaps beneath the flows provide the smooth and nearly continuous subsurface interface that allows for a strong subsurface return [13]. Although the permittivity of the basalt lava flows is high, a 68-cm radar wave is able to penetrate a few centimeters and reflect from the boundary between the flow and internal air gaps. The dielectric contrast between the lava and air is high, and the upper and basal interfaces involved are very smooth at the wavelength scale.

One terrestrial example that may involve a scenario more like Fig. 1(c) is an area near Sunset Crater, AZ [13], where a high degree of linear polarization is associated with a few specific radar-dark cinder and ash deposits. Field observations of one such cinder cone reveal centimeter-scale cinders as well as meter-scale blocks covering the ground and partially buried in a soil and ash matrix that slopes smoothly away from the cinder cone. Larger blocks are located closer to the base of the cone, where the degree of linear polarization is higher. In this instance, the radar wave may reflect from the large blocks buried in the soil matrix.

These terrestrial examples demonstrate that in all of the currently identified cases where a significant degree of linear polarization is observed, the upper surface is smooth at the wavelength scale. A detectable degree of linear polarization value also appears to require abundant subsurface reflectors with relatively strong dielectric contrast with the covering layer or surrounding medium.

IV. VENUS

Arecibo observations from 1999 through 2004 produced images of the hemisphere of Venus visible from Earth at inferior conjunction, at resolutions of 12 and 16 km. These regional data show that areas with a high degree of linear polarization are concentrated in discrete areas, or “features.” These features correspond to impact crater ejecta, lava flows, dome fields, and aeolian settings [12], [13]. In this section, we include a new analysis of the circular polarization ratio to better understand the types of surfaces that are present in volcanic and impact cratering settings.

Distal impact crater ejecta deposits, including parabola-shaped features surrounding some craters [10], account for many of the local increases in the degree of linear polarization. In most cases, these correspond to areas of slightly increased radar backscatter, as is the case with the Carson crater parabola [12]. In these cases, the radar bright terrain mostly likely reflects subsurface scattering from larger blocks embedded in fine-grained ejecta material [e.g. Fig. 1(c), (e), or (f)].

In other cases, such as the radar dark halos surrounding the craters Galina (Fig. 3) and Shih Mai-Yu, high m_l values correspond to areas with a low backscatter cross section.

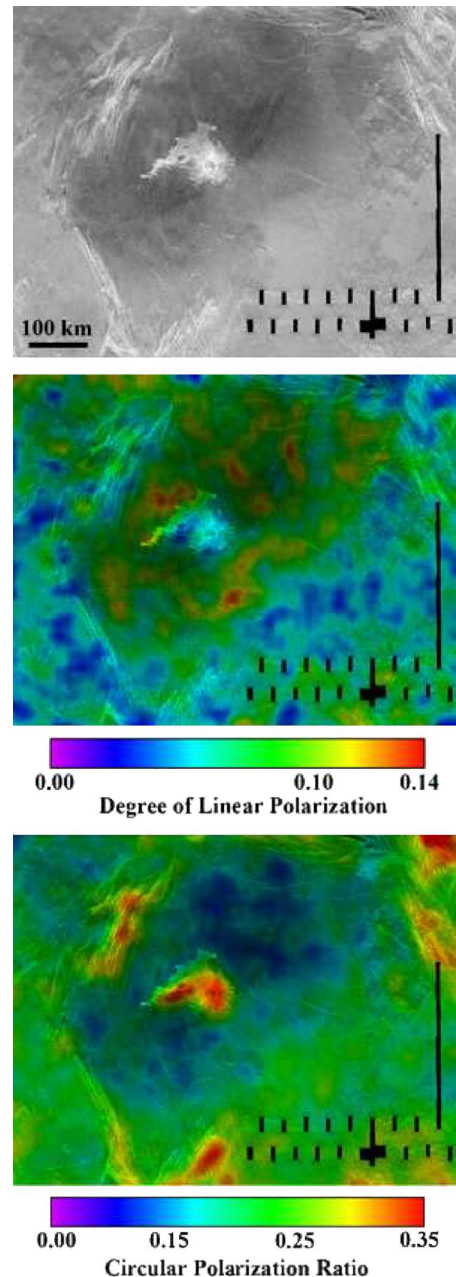


Fig. 3. Images of Galina crater (47.6° N, 307.1° E) on Venus. Top: Magellan synthetic aperture radar (SAR) image showing the dark halo surrounding the crater. Middle: A degree of linear polarization image stretched to a color scale and overlaid on the Magellan image. The radar dark halo has larger degree of linear polarization values than surrounding areas of radar-bright plains. Bottom: A circular polarization ratio image stretched to a color scale and overlaid on the Magellan image. The radar dark halo surrounding the crater has a low circular polarization ratio, similar to dark halos that surround some lunar craters [18].

On the Moon, radar-dark halos with low circular polarization ratios surround young craters, and are caused by a zone of fine-grained pulverized material that falls near the impact site [18], [19]. Over time, these radar-dark zones

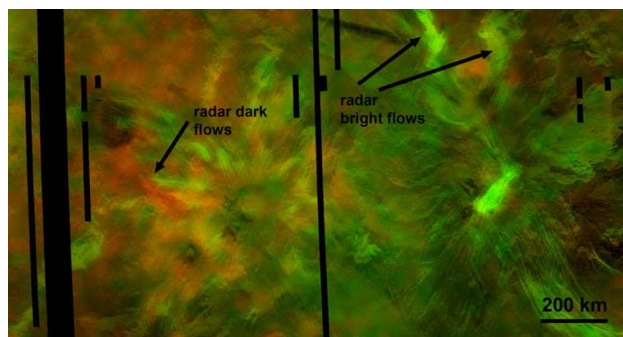


Fig. 4. An image of Sif and Gula Mons (center 40.4° N, 353.7° E) showing both degree of linear polarization (red) and circular polarization ratio (green) overlaid on a Magellan SAR image. Both polarizations were stretched with a linear scale such that runs from zero to twice the average value across the scene. For the degree of linear polarization, the range is 0–0.11. For the circular polarization ratio the range is 0–0.31. Areas with a higher-than-average degree of linear polarization, and a lower-than-average circular polarization ratio, are the most red. Areas close to the average for both polarization products are yellow. Green areas have a lower-than-average degree of linear polarization and an above-average circular polarization ratio. Displaying both polarization products simultaneously illustrates the complexity and variety of different surfaces present in volcanic areas on Venus.

become mixed with larger blocks, and the distinctive low circular polarization ratio ring disappears [18]. As can be seen in Fig. 3, the Galina halo has a low μ_c , as is the case for the lunar craters. In the case of these dark halo deposits on Venus, the radar wave may travel into a smooth, fine-grained deposit and reflect from a gently undulating, buried interface [e.g., Fig. 1(b)]. If large quantities of buried blocks were present, it is likely that a higher circular polarization ratio would be observed.

Some volcanic settings also show an enhanced degree of linear polarization, including both shield fields and lava flows. Fig. 4 shows the degree of linear polarization (red) and the circular polarization ratio (green) overlaid on a Magellan image of Sif and Gula Montes. It is clear from this image that different lava flows have different physical properties. Radar dark lava flows on the flank of Sif Mons show a higher degree of linear polarization than most other flows in the vicinity [13]. It is possible that in these cases, gaps within the flows may be causing the increased degree of linear polarization values, similar to the Kilauea example discussed in Section III [Fig. 1(b)]. Radar bright flow complexes north of Gula Mons have high circular polarization ratio values, indicating that they likely have a surface that is mostly rough with little appreciable surface coating [Fig. 1(d)]. Even within these bright flows, however, it is possible to see color variations due to the changing polarization values that indicate changing surface roughness and radar penetration. The flanks of Sif Mons have a greater area of increased linear polarization than the flanks of Gula Mons, suggesting that there is more

overall surface mantling across Sif Mons. It is not possible to be certain what causes this difference, but there may be fine volcanic material across much of Sif Mons, or perhaps recent cratering events on or east of Sif Mons deposited impact ejecta across the edifice.

The highest degrees of linear polarization are confined to local areas, but we detect a measurable (i.e., above the expected spurious few percent due to calibration uncertainties) amount of linearly polarized echo across most of the Venusian surface. Perhaps the best illustration of this is the linear polarization angle maps. Figs. 5 and 6 show the northern and southern hemispheres of Venus, respectively, from data acquired in 2001. The degree of linear polarization values are low near the subradar point where the incidence angle is small, and increase towards the limbs as the incidence angle increases. Close to the subradar point where degree of linear polarization values are expected to be very small [(3) and (4)], it can be difficult to discern whether subsurface scattering still occurs and whether specific features are present. Nonrandom values in the polarization angle maps demonstrate that even at low incidence angles, some fraction of the echo power is returned from the subsurface, and that the slight regional increases in the degree of linear polarization are associated with specific geologic structures.

The linear polarization angle rotates across the surface of the planet as the plane of incidence and reflection changes across the sphere, as discussed in Section II. The discrete surface features visible in the degree of linear polarization maps have consistent linear polarization angle values, and a quantitative but relative comparison of the χ values for different features demonstrates that the linear polarization angles rotate in step with the change in the plane of incidence caused by the planetary curvature [13].

The maps in Figs. 5 and 6 show that large portions of the Venus surface have some component of subsurface scattering at 12.6-cm wavelength. This suggests that while large and continuous surficial deposits occur mostly in local areas on Venus, there may be a broadly distributed background of patchy, penetrable surface materials such as dust or regolith. These deposits could be very thin (centimeter scale), so it is not clear that the data imply significant additional fine-grained surface materials. However, it does suggest that patchy coatings may be more common than thought based on analysis of Magellan radar images, which cannot distinguish subtle variations in such thin surface coatings from minor changes in surface roughness.

Many of the high degree of linear polarization features, including the high radar reflectivity summits of Tepev and Theia Montes, correspond fully or partially to areas with lower than the Venus average emissivity value of 0.84 [27]. Low emissivity areas have generally been attributed to an increase in the dielectric constant [27], although volume scattering in a low-loss medium could also be responsible [33]. A higher surface dielectric constant can lead to a larger m_l value (Section II), but it can also increase the

surface echo component and decrease the fraction of the echo that comes from subsurface scattering. A small decrease in the Magellan emissivity could be caused by a change in surface roughness, which may explain the low emissivity and high m_l correlations in the case of distal crater ejecta. If the surface is smooth, then the Magellan data measure the true H -polarized emissivity, which is less than that of a rougher surface [4].

In some instances, particularly Stuart crater and the Tepev and Theia Montes summits, the emissivity values are too low to be explained through surface roughness variations. The floor of Stuart crater has an emissivity of 0.69 and a high degree of linear polarization (Fig. 7). Stuart is the only example where high m_l values are associated with the interior of a crater; the rough surface of the crater floor and walls should generally preclude any

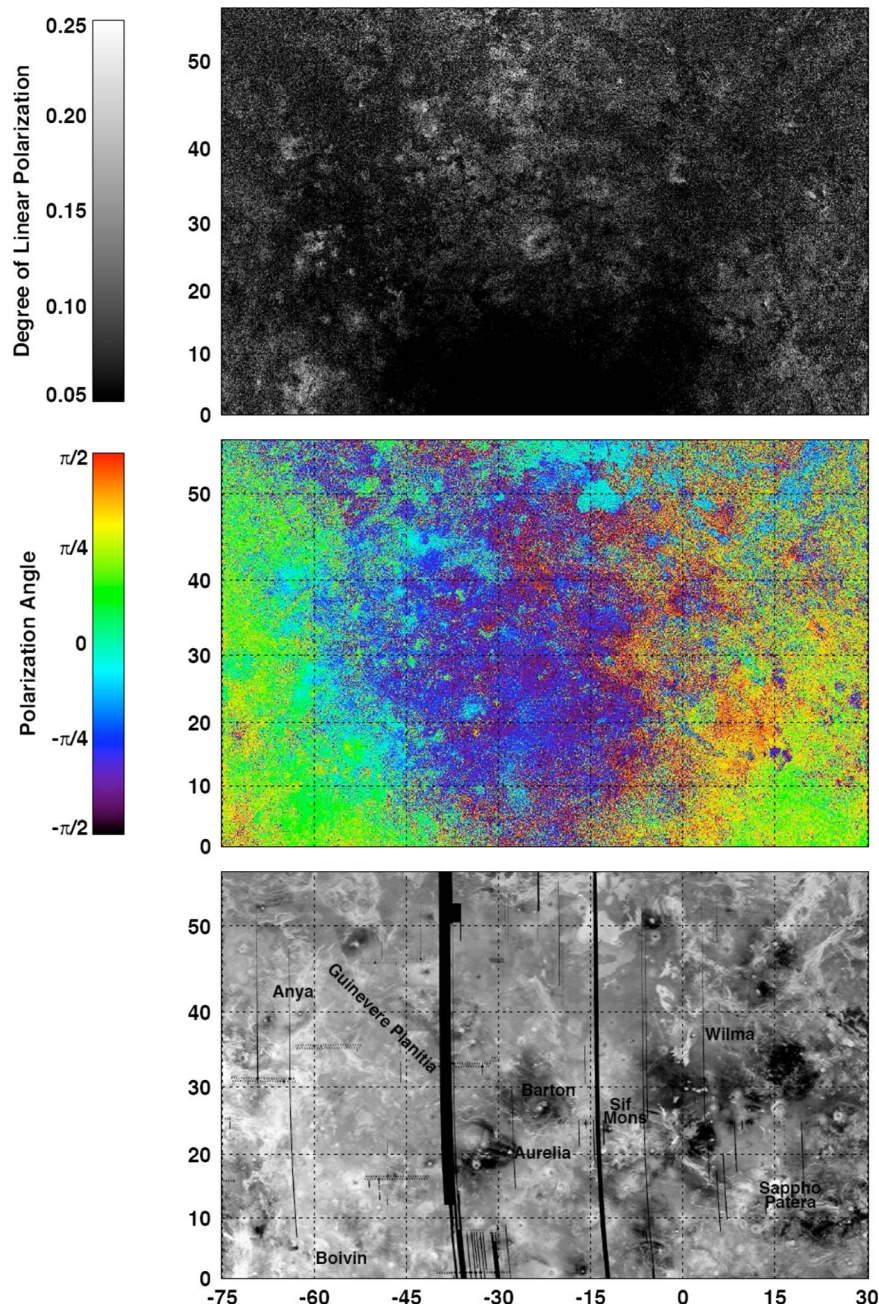


Fig. 5. Maps of the northern hemisphere of Venus, from data obtained in 2001. The subradar point is in the lower center of the image. Incidence angle increases away from the subradar point, towards the top and sides of the image. **Top:** The degree of linear polarization image. **Middle:** The linear polarization angle. This angle rotates as the plane of incidence and reflection (perpendicular to the surface) rotates with the curvature of the planet. **Bottom:** A Magellan SAR image with features labeled for reference.

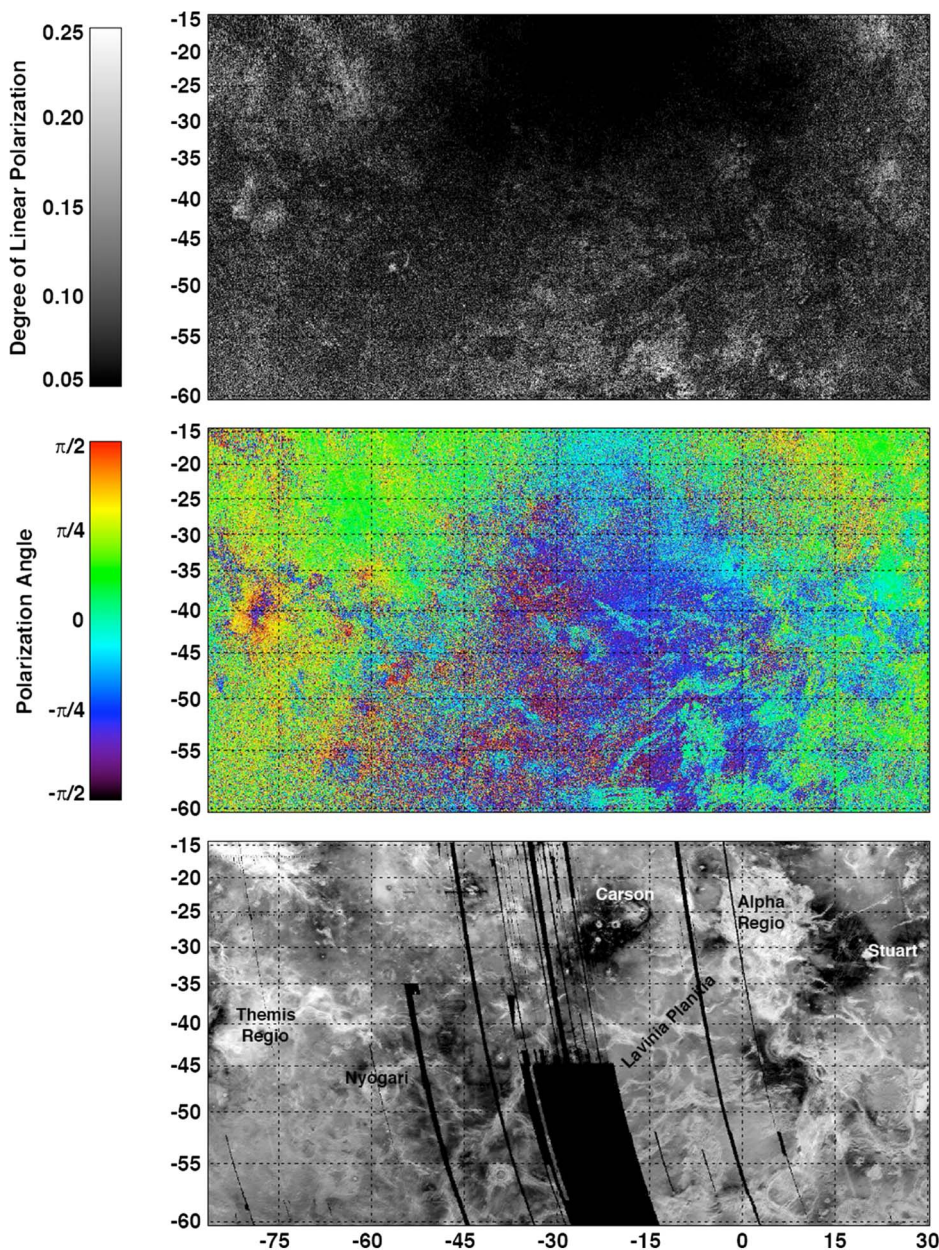


Fig. 6. Maps of the southern hemisphere of Venus, from data obtained in 2001. The subradar point is in the upper center of the image. Incidence angle increases away from the subradar point, towards the bottom and sides of the image. Top: The degree of linear polarization image. This angle rotates as the plane of incidence and reflection (perpendicular to the surface) rotates with the curvature of the planet. Middle: The linear polarization angle. Bottom: A Magellan SAR image with features labeled for reference.

strong echo from subsurface scattering. Indeed, the circular polarization ratio image demonstrates that the interior of the crater is rough. The combination of polarization behaviors suggests a scenario like Fig. 1(e) or (f). However, it is still not clear how an area with a significant surface cover of low density material could have such a low emissivity. In the case of the high-reflectivity, low-emissivity summit regions, perhaps the radar wave is able to penetrate into high dielectric materials in small areas with a very smooth surface texture. Alternatively, there may be

thin, unresolved patches of surface coatings across some parts of the high-dielectric-constant regions. Higher resolution polarimetric imaging or emissivity, radar images at a different wavelength, or surface images would all help to differentiate between these cases.

V. MOON

Lunar data at both S- and P-band wavelength (12.6 and 70 cm, respectively) have been obtained using the Arecibo

Observatory radar transmitter and the Green Bank Telescope as a receiver [7], [9]. These data sets have a much higher resolution (20–80 m/pixel at S-band) than the Venus data, and therefore have the potential to show finer details in areas of geologic interest.

Preliminary work using the lunar Stokes vector data has focused on volcanic terrains. The Aristarchus region of the Moon is an uplifted plateau that has been the site of extensive volcanism. A large rille emanates from the Cobra Head source vent, and the plateau is mantled in thick pyroclastic deposits that cover an area of $\sim 49\,000\text{ km}^2$ [17]. S-band images (Fig. 8) show radar-dark, lobate, slumping terrain surrounding the head of the rille. Radar-bright streaks cross some areas of the pyroclastic

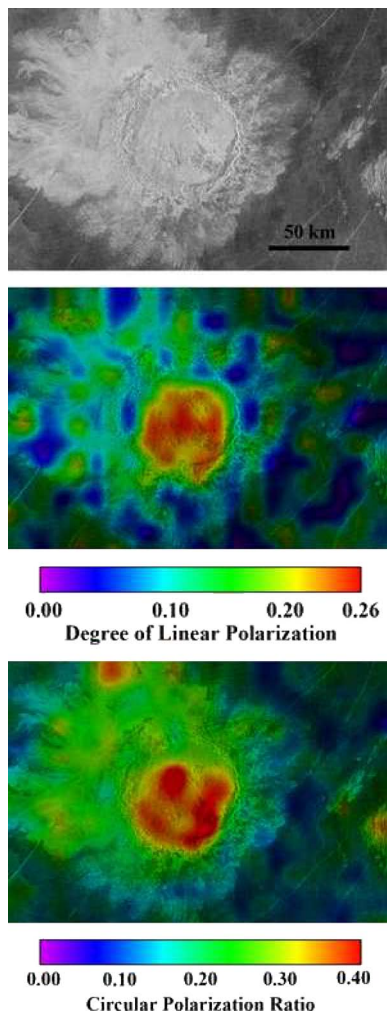


Fig. 7. Images of Stuart crater ($30.8^\circ\text{ S}, 20.2^\circ\text{ E}$), Venus. Top: A Magellan SAR image. Middle: A degree of linear polarization image that has been stretched to a color scale and overlaid on the Magellan image. In this case, a high degree of linear polarization is observed from within the crater walls. Bottom: A circular polarization ratio image that has been stretched to a color scale and overlaid on the Magellan image. The crater floor has a high circular polarization ratio, suggesting a rough surface or subsurface.

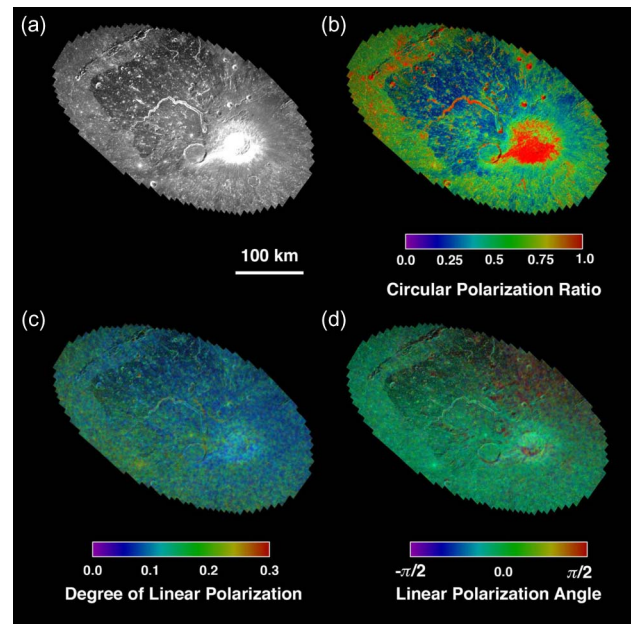


Fig. 8. Polarimetric data of Aristarchus plateau. The radar bright Aristarchus crater is located at 23.7° N and 47.4° E . (a) Total power image. (b) Circular polarization ratio stretched to a color scale and overlaid on the total power image. (c) Degree of linear polarization, smoothed, stretched to a color scale, and overlaid on the total power image. (d) Linear polarization angle, smoothed, stretched to a color scale, and overlaid on the total power image.

deposit and mark deposits of blocky material from the Aristarchus impact. In corresponding P-band images, some areas of the deposit have a higher radar backscatter, and Campbell *et al.* [8] propose that the pyroclastic material is covering lava flows that lie, at most, 15 m below the surface. The same areas are slightly brighter at S-band as well, probably because impacts have penetrated the deposit and mixed blocky material into the pyroclastics [8].

Images of the circular polarization ratio, degree of linear polarization, and linear polarization angle are shown in Fig. 8, from data acquired at 40-m/pixel single-look resolution. The degree of linear polarization and linear polarization angle data were averaged to 800-m/pixel resolution to reduce speckle before being overlaid on the total power image [Fig. 8(c) and (d)]. The pyroclastic materials are radar dark and have a very low circular polarization ratio, most likely because they are smooth, fine-grained, and block free. The circular polarization ratio overlay clearly highlights the difference between fine-grained pyroclastics and the higher circular polarization ratio impact crater ejecta.

The degree of linear polarization image, however, shows little correlation with the circular polarization ratio image; the high μ_c value streaks do not uniformly match with high or low m_l values, and the buried lava flow shown in [8] is not visible in the linear polarization data. The crater Aristarchus has a low degree of linear polarization,

as might be expected for a rough, blocky surface, but other craters, including the large crater Herodotus, have average m_l values. Aristarchus has a radar-dark halo in 70-cm wavelength ground-based radar images [18] that can also be seen in the S-band (Fig. 8) data, although it is somewhat subdued. However, there is no corresponding increase in the degree of linear polarization in the S-band data [Fig. 8(c)], as is seen for some of the Venus craters. The pyroclastic deposit itself has a degree of linear polarization value of around 0.14, which is identical to the surrounding mare basalts. Fig. 8(c) has fairly uniform values across large portions of the scene, with some of the minor fluctuations probably due to statistical errors of ~ 0.04 due to S_2 and S_3 noise and other errors as discussed in Section II.

The linear polarization angle image shown in Fig. 8(d) covers a much smaller area than the Venus maps in Figs. 5 and 6, and therefore does not show large angle changes due to the curvature of the Moon. Instead, the image shows that the value of χ changes as the plane of incidence and reflection changes with topography around crater rims. The linear polarization angle image also shows a large area to the northeast with different angle values (colored red), which probably represents a large plateau-forming block that has been tilted along a fault.

The uniform value of degree of linear polarization across the Aristarchus pyroclastic suggests that the radar wave may penetrate into the surface and reflect from buried objects almost everywhere in the image. Other lunar data, such as an area near the crater Focas on the western limb of the Moon [9], and the Cauchy dome field in Mare Tranquillitatis, also show a nearly uniform degree of linear polarization across the image despite the presence of various-aged impact craters and volcanic structures. In the case of the Moon, the ubiquitous regolith covering may provide an adequate medium for a significant component of subsurface scattering of a 12.6-cm wave in most situations, with the absolute value of the back-scattered power modulated by the volume population of wavelength-scale rocks within the probing depth of the signal.

While the change in degree of linear polarization values across the lunar images is less pronounced than for Venus, the minimum and maximum m_l values at a given incidence angle are roughly similar. For example, parts of the Aristarchus pyroclastic (image center $\theta = 53^\circ$) have m_l values of about 0.05, and the radar bright Aristarchus ejecta have m_l values of 0.09, so there are some localized patches where little echo power is returned from the subsurface. At higher incidence angles, such as the Focas crater example (center $\theta = 88^\circ$) [9], the average degree of linear polarization reaches values of up to 0.3, which is similar to some examples on Venus. At S-band wavelength, the major difference between the two bodies appears to be the higher “background” fraction of subsurface scatter from the lunar regolith.

VI. DISCUSSION AND CONCLUSION

Radar data processed using the dual-polarimetry Stokes parameter technique demonstrate some clear differences among planetary surfaces. In the case of the Moon, a thick regolith covering with suspended rocks appears to generate a fairly uniform degree of linear polarization. In contrast, on Venus, and in terrestrial cases like those discussed in Section III, the degree of linear polarization is typically low for most surfaces, and is enhanced only for certain well-defined features such as layered lava flows and smooth dust- or sand-covered areas. On both the Moon and Venus, the circular polarization ratio varies significantly as the surface roughness and subsurface block abundance change between local geologic units.

Since the local behavior of the degree of linear polarization is so different for the Moon and Venus, it is interesting to compare the incidence angle trends of the degree of linear polarization to determine the global behavior of this parameter. A simple model for the degree of linear polarization assumes a single-layer model like that shown in Fig. 1(b), with a fine-grained surface coating overlying a quasi-specular subsurface scattering layer. In this case, the degree of linear polarization depends solely on the transmission coefficients in (3) and (4) [29]. To some extent, this model provides an upper limit, because power loss through the surface layer, and increased diffuse

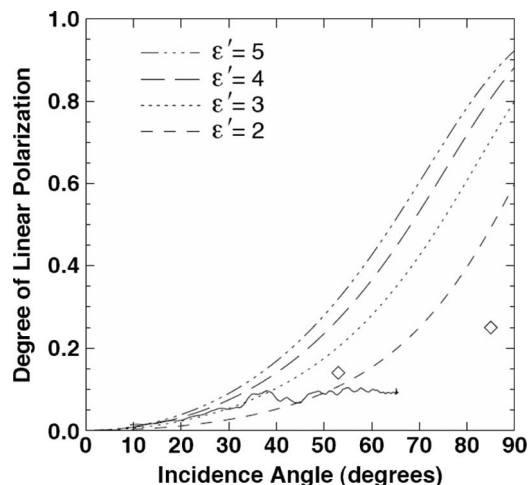


Fig. 9. Plots of a simple scattering model for the degree of linear polarization shown with Venus data (solid line) and lunar measurements (diamonds). In this model, the radar wave penetrates into a surface that is smooth at the wavelength scale and reflects in a quasi-specular fashion from a subsurface interface. The model is plotted for different values of the mantling (surface) layer dielectric constant. The Venus data line is an average derived from northern hemisphere data acquired in 2001. The increased values around 36° incidence are the result of a polarization feature surrounding Barton crater; individual features typically have a higher than average degree of linear polarization. The lunar data are averages acquired away from large impact craters for the Aristarchus and Focas scenes.

scattering from the surface or subsurface, will both lower the degree of linear polarization values across all incidence angles. Fig. 9 shows the predicted scattering behavior for this model, which predicts high m_l values at moderate to large angles of incidence.

The actual behaviors for the Moon and Venus, also plotted in Fig. 9, show that the background degree of linear polarization values averaged across Venus are fairly low out to 70° incidence. Areas near the edges of the Venus images have increased statistical and systematic errors due to decreased signal-to-noise ratio and are not plotted, but m_l values averaged over large areas are still less than the ~ 0.3 predicted for low-dielectric constant materials (e.g., see Figs. 5 and 6). Average m_l values for individual Venus features are larger than the background, presumably because a larger fraction of the surface is covered in mantling material; however, the m_l values are still low at higher incidence angles. For example, an area near the crater Xantippe (62° incidence) has an average value around 0.25. The highest m_l values measured for individual pixels within specific features are still lower than 0.35. The Moon displays a similar behavior, although the polarimetric analysis is still in early stages and so only points from a few analyzed scenes are available. At high incidence angles, for example near-limb areas near Mare Orientale and Focas crater ($\theta \sim 80^\circ\text{--}85^\circ$), the average degree of linear polarization values are ~ 0.25 .

It is clear that the simple model shown in Fig. 9 does not entirely explain the scattering regime leading to high m_l values. At moderate incidence angles ($30^\circ\text{--}40^\circ$), the model roughly matches the average measured degree of linear polarization values, but as the incidence angles ex-

ceed 50° , the model is less reasonable. The average permittivity of the lunar regolith is 2.8 [11], and at high incidence angles, the measured degree of linear polarization values would suggest a surface material with an even lower permittivity. Instead, changes in the relative amounts of surface and subsurface scattering, and incidence angle related changes in the relative amount of quasi-specular and diffuse scattering, likely contribute to the incidence angle behavior of the measured fraction of linear-polarized echo power.

In summary, radar polarimetry has the capability to better distinguish between different types of surface and subsurface physical properties than single-polarization radar imagery, and can be useful for comparing scattering regimes across planetary objects. Future modeling using high-resolution data, such as the terrestrial and lunar data sets, will help to better understand the types of surfaces that produce different combinations of polarimetric behaviors. Additional comparisons with radiometric data will be useful to better understand why the high degree of linear polarization features on Venus are often correlated with low microwave emissivity. SAR systems designed for future planetary missions will benefit greatly from including polarimetric capabilities. ■

Acknowledgment

The authors would like to thank the staff of the Arecibo and Green Bank Observatories for their help with the observations discussed in this paper. Three anonymous reviewers and N. J. S. Stacy provided helpful comments that improved the manuscript.

REFERENCES

- [1] B. A. Campbell, S. H. Zisk, and P. J. Mouginis-Mark, "Lunar surface scattering from new 3-cm polarization and phase radar data," in *Proc. Lun. Plan. Sci. Conf.*, XIX, 1988, p. 161.
- [2] B. A. Campbell, J. F. Bell, III, S. H. Zisk, B. R. Hawke, and K. A. Horton, "A high-resolution radar and CCD imaging study of crater rays in mare serenitatis and mare nectaris," in *Proc. Lun. Plan. Sci. Conf.*, 1992, vol. 22, pp. 259–274.
- [3] B. A. Campbell and D. B. Campbell, "Analysis of volcanic surface morphology on Venus from comparison of Arecibo, Magellan, and terrestrial airborne radar data," *J. Geophys. Res.*, vol. 97, pp. 16 293–16 314, 1992.
- [4] B. A. Campbell, "Merging Magellan emissivity and SAR data for analysis of Venus dielectric properties," *Icarus*, vol. 112, pp. 187–203, 1994.
- [5] B. A. Campbell, T. A. Maxwell, and A. Freeman, "Mars orbital synthetic aperture radar: Obtaining information from radar polarimetry," *J. Geophys. Res.*, vol. 109, E07008, 2004, DOI: 10.1029/2004JE002264.
- [6] B. A. Campbell and B. R. Hawke, "Radar mapping of lunar cryptomare east of Orientale basin," *J. Geophys. Res.*, vol. 110, E09002, 2005, DOI: 10.1029/2005JE002425.
- [7] B. A. Campbell, D. B. Campbell, J. L. Margot, R. R. Ghent, M. Nolan, J. Chandler, L. M. Carter, and N. J. S. Stacy, "Focused 70-cm mapping of the moon," *IEEE Trans. Geosci. Remote Sens.*, vol. 45, no. 12, pt. 2, pp. 4032–4042, Dec. 2007.
- [8] B. A. Campbell, L. M. Carter, B. R. Hawke, D. B. Campbell, and R. R. Ghent, "Volcanic and impact deposits of the moon's Aristarchus plateau: A new view from earth-based radar images," *Geology*, vol. 36, pp. 135–138, 2008.
- [9] B. A. Campbell, L. M. Carter, D. B. Campbell, M. C. Nolan, J. Chandler, R. R. Ghent, B. R. Hawke, R. F. Anderson, and K. S. Wells, "S-band radar mapping of the moon with the Arecibo and green bank telescopes," *Icarus*, vol. 208, pp. 565–573, 2010.
- [10] D. B. Campbell, N. J. S. Stacy, W. I. Newman, R. E. Arvidson, E. M. Jones, G. S. Musser, A. Y. Roper, and C. Schaller, "Magellan observations of impact crater related features on the surface of Venus," *J. Geophys. Res.*, vol. 97, pp. 16 249–16 277, 1992.
- [11] W. D. Carrier, G. R. Ohloeff, and W. Mendell, "Physical properties of the lunar surface," in *Lunar Sourcebook*. New York: Cambridge Univ. Press, 1991, pp. 475–567.
- [12] L. M. Carter, D. B. Campbell, and B. A. Campbell, "Impact crater related surficial deposits on Venus: Multipolarization radar observations with Arecibo," *J. Geophys. Res.*, vol. 109, E06009, 2004, DOI: 10.1029/2003JE002227.
- [13] L. M. Carter, D. B. Campbell, and B. A. Campbell, "Volcanic deposits in shield fields and highland regions on Venus: Surface properties from radar polarimetry," *J. Geophys. Res.*, vol. 111, E06005, 2006, DOI: 10.1029/2005JE002519.
- [14] J. V. Evans and G. H. Pettengill, "The scattering behavior of the moon at wavelengths of 3.6, 68, and 784 centimeters," *J. Geophys. Res.*, vol. 68, pp. 423–447, 1963.
- [15] J. V. Evans, R. P. Ingalls, R. P. Rainville, and R. R. Silva, "Radar observations of Venus at 3.8 cm wavelength," *Astronom. J.*, vol. 71, pp. 902–915, 1966.
- [16] J. V. Evans and T. Hagfors, "Study of radio echoes from the moon at 23 centimeter wavelength," *J. Geophys. Res.*, vol. 71, pp. 4871–4899, 1966.
- [17] L. R. Gaddis, M. I. Staid, J. A. Tyburczy, B. R. Hawke, Noah, and E. Petro, "Compositional analyses of lunar pyroclastic deposits," *Icarus*, vol. 161, pp. 262–280, 2003.
- [18] R. R. Ghent, D. W. Leverington, B. A. Campbell, B. R. Hawke, and D. B. Campbell, "Earth-based observations of radar-dark crater haloes on the moon: Implications for regolith properties,"

- J. Geophys. Res.*, vol. 110, E02005, 2005, DOI: 10.1029/2004JE002366.
- [19] R. R. Ghent, V. Gupta, B. A. Campbell, S. A. Ferguson, J. Brown, R. Ferguson, and L. M. Carter, "Generation and atmospheric entrainment of fine-grained ejecta in planetary impacts," *Icarus*, 2010, DOI: 10.1016/j.icarus.2010.05.005.
- [20] R. M. Goldstein, "Preliminary Venus radar results," *J. Res. NBS*, vol. 69D, pp. 1623–1625, 1965.
- [21] R. Greeley, D. G. Blumberg, J. F. McHone, A. Dobrovolskis, J. D. Iverson, N. Lancaster, K. R. Rasmussen, S. D. Wall, and B. R. White, "Applications of spaceborne radar laboratory data to the study of aeolian processes," *J. Geophys. Res.*, vol. 102, pp. 10 971–10 983, 1997.
- [22] T. Hagfors and D. B. Campbell, "Radar backscattering from Venus at oblique incidence at a wavelength of 70 cm," *Astronom. J.*, vol. 79, pp. 493–502, 1974.
- [23] T. Hagfors, R. A. Brockelman, H. H. Danforth, L. B. Hansen, and G. M. Hyde, "Tenuous surface layer on the moon: Evidence derived from radar observations," *Science*, vol. 150, pp. 1153–1156, 1965.
- [24] J. D. Jackson, *Classical Electrodynamics*, 3rd ed. Hoboken, NJ: Wiley, 1999.
- [25] G. S. Levi and D. Schuster, "Further Venus radar depolarization experiments," *Astronom. J.*, vol. 69, pp. 29–33, 1964.
- [26] S. Nozette, P. Spudis, B. Bussey, R. Jensen, K. Raney, H. Winters, C. L. Lichtenberg, W. Marinello, J. Crusan, M. Gates, and M. Robinson, "The lunar reconnaissance orbiter miniature radio frequency (mini-RF) technology demonstration," *Space Sci. Rev.*, vol. 150, pp. 285–302, 2010.
- [27] G. H. Pettengill, P. G. Ford, and R. J. Wilt, "Venus radiothermal emission as observed by Magellan," *J. Geophys. Res.*, vol. 97, pp. 13091–13102, 1992.
- [28] R. K. Raney, "The lunar mini-RF radars: Hybrid polarimetric architecture and initial results," *IEEE Trans. Geosci. Remote Sens.*, 2010.
- [29] N. J. S. Stacy, "High resolution synthetic aperture radar observations of the Moon," Ph.D. dissertation, Dept. Astronom., Cornell Univ., Ithaca, NY, 1993.
- [30] N. J. S. Stacy and D. B. Campbell, "Stokes vector analysis of lunar radar backscatter," in *Proc. Int. Geosci. Remote Sens. Symp.*, 1993, pp. 30–32.
- [31] N. J. S. Stacy, D. B. Campbell, and P. G. Ford, "Arecibo radar mapping of the lunar poles: A search for ice deposits," *Science*, vol. 276, pp. 1527–1530, 1997.
- [32] T. W. Thompson, B. A. Campbell, R. R. Ghent, B. R. Hawke, and D. W. Leverington, "Radar probing of planetary regoliths: An example from the northern rim of Imbrium basin," *J. Geophys. Res.*, vol. 111, E06S14, 2006, DOI: 10.1029/2005JE002566.
- [33] K. A. Tryka and D. O. Muhleman, "Reflection and emission properties on Venus: Alpha Regio," *J. Geophys. Res.*, vol. 97, pp. 13379–13394, 1992.
- [34] J. J. Van Zyl, H. A. Zebker, and C. Elachi, "Imaging radar polarization signatures: Theory and observations," *Radio Sci.*, vol. 22, pp. 529–543, 1987.
- [35] K. S. Wells, D. B. Campbell, B. A. Campbell, and L. M. Carter, "Detection of small lunar secondary craters in circular polarization ratio radar images," *J. Geophys. Res.*, vol. 115, E06008, 2010, DOI: 10.1029/2009JE003491.
- [36] S. H. Zisk, P. J. Mouginiis-Mark, G. H. Pettengill, and T. W. Thompson, "New very high resolution lunar radar measurements at 3 cm wavelength: Maps of the Hadley/Apollo 15 area," in *Proc. Lun. Plan. Sci. Conf.*, XVIII, 1987, p. 1130.

ABOUT THE AUTHORS

Lynn M. Carter received the B.S. degree in astronomy and physics from the University of Illinois at Urbana-Champaign, Urbana, in 1999 and the Ph.D. degree in astronomy from Cornell University, Ithaca, NY, in 2005.

She was a Postdoctoral Researcher with the Center for Earth and Planetary Studies, Smithsonian Institution, Washington, DC, from 2004 to 2010. Currently, she is a Research Scientist at the NASA Goddard Space Flight Center, Greenbelt, MD. Her primary research interest is planetary geology, particularly the composition and structure of the surface of Venus, Mars, the Moon, Titan, and asteroids. She is a team member on the SHARAD shallow radar sounder on Mars Reconnaissance Orbiter and a participating scientist on the Mini-RF radar on Lunar Reconnaissance Orbiter. Her current research projects include ground- and space-based radar studies of lunar volcanism and impact cratering, studies of lava flows and plains stratigraphy using the SHARAD radar, and planetary analog and ground-penetrating radar studies of volcanic terrains.



Donald B. Campbell received the B.S. and M.S. degrees in physics from the University of Sydney, Sydney, Australia and the Ph.D. degree in astronomy and space sciences from Cornell University, Ithaca, NY, in 1971.

His primary research involves the study of the radio wavelength scattering properties of solid surfaces in the solar system. Much of this work has been carried out using the radar systems on the 305-m Arecibo telescope. He used the first, 70-cm wavelength, radar system on the Arecibo telescope to obtain some of the early images of the surface of Venus utilizing interferometry to resolve ambiguity problems and, later, the then new 13-cm wavelength high-



powered radar system on the telescope to obtain the first high-resolution imagery of the planet's surface. This was followed by participation as a coinvestigator on the Magellan orbiting radar mission to Venus. Campbell, working with his collaborators, made the first radar detections of the icy satellites of Jupiter discovering the unusual radar scattering properties of low-temperature water ice surfaces. More recently, working with graduate students and collaborators, he has been involved in multipolarization studies of the radar echoes from Venus, the Moon, and the satellites and rings of Saturn. Most of his professional career has been with Cornell University, initially on the research staff of the Arecibo Observatory where he served as the observatory's Director in the 1980s. In January 1988, he was appointed Professor of Astronomy at Cornell University and also served as Associate Director of the National Astronomy and Ionosphere Center (NAIC), which operates the Arecibo Observatory, from 1993 to 2004. In 2008, he was appointed Director of NAIC, a position that he still holds.

Bruce A. Campbell received the B.S. degree in geophysics from Texas A&M University, College Station, in 1986 and the Ph.D. degree in geology and geophysics from the University of Hawaii, Honolulu, in 1991.

He joined the staff of the Center for Earth and Planetary Studies, Smithsonian Institution, Washington, DC, in 1992. From 1996 to 1998, he was the Discipline Scientist for NASA's Planetary Instrument Definition and Development Program. His research interests focus on applications of radar remote sensing to the understanding of volcanism, impact cratering, weathering, and other surficial processes on the terrestrial planets. He is a team member for the SHARAD shallow radar sounder on the Mars Reconnaissance Orbiter.

